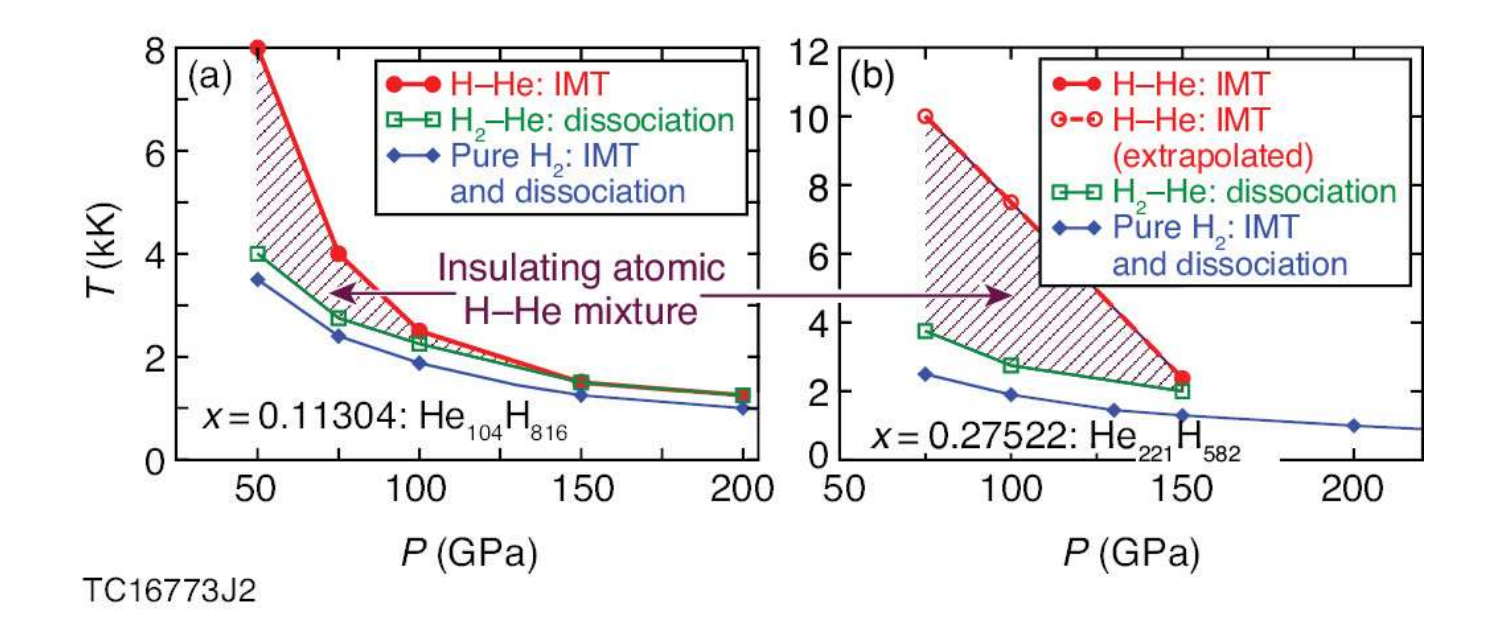
Exchange-Correlation Free-Energy density Functionals: Recent Developments and Applications





V. V. Karasiev University of Rochester Laboratory for Laser Energetics

Strongly Coupled Coulomb Systems
Tahoe Blue Event Center
Stateline, NV
July 27 – August 01, 2025



Collaborators



S. X. Hu, K.P. Hilleke, D. I. Mihaylov, A. Ellaboudy

University of Rochester Laboratory for Laser Energetics

- A. Bergermann, R. Redmer
 - B. Universität Rostock
- S. B. Trickey and J. W. Dufty

University of Florida

Funding Acknowledgments

This work was supported by U.S. National Science Foundation PHY Grant No. 2205521

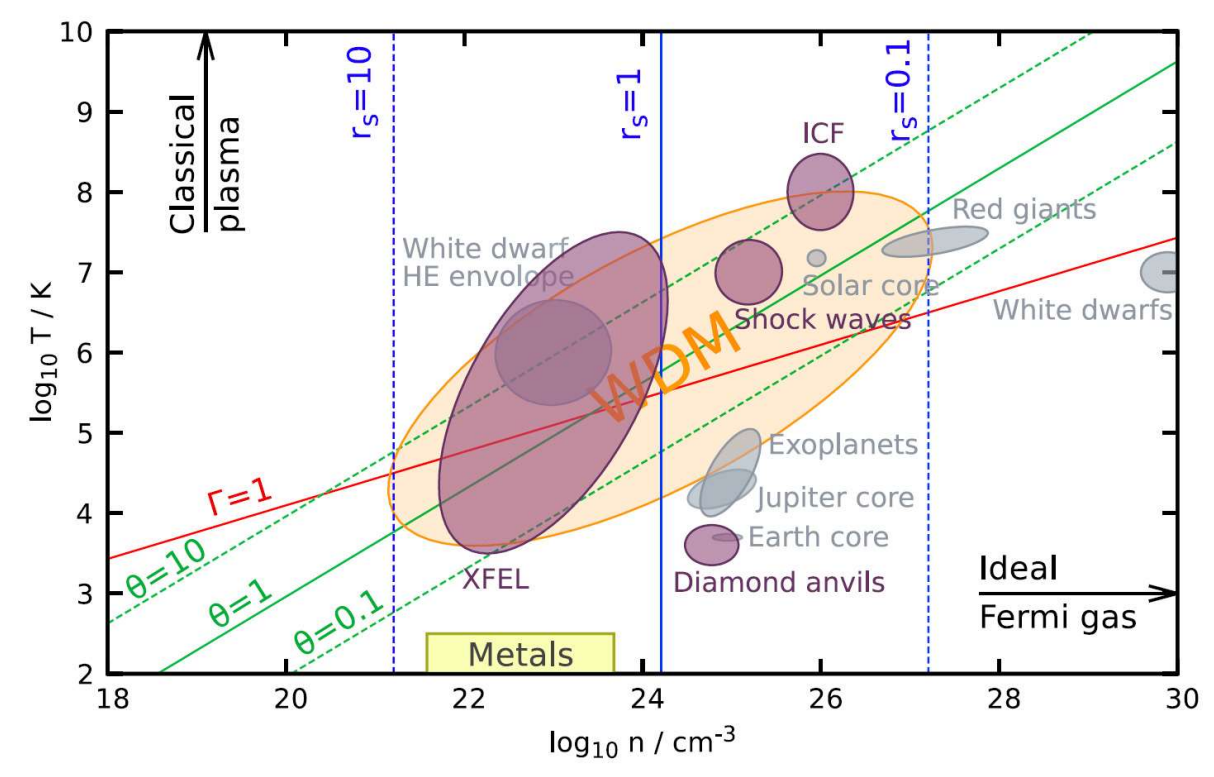
This material is based upon work supported by the Department of Energy National Nuclear Security Administration under Award Number DE-NA0004144.



Motivation

Our goal is to develop more accurate XC free-energy density functionals for a better description of warm dense matter and dense plasma properties





- Classical plasma approaches work only for weakly coupled nondegenerate systems (Γ << 1: low density, very high temperature)
- •All regions except left upper corner require quantum treatment of electronic degrees of freedom

Schematic temp.-density diagram (T. Dornheim et al., Phys. Rep 744, 1 (2018))

ICF: inertial confinement fusion



DFT-based AIMD allows for calculations of many material properties required for simulations of ICF implosions and provides predictions for HEDP experiments



Some of material properties accessible from DFT-based AIMD simulations

- Equation of state
- Phase transitions
- Thermal conductivity
- Electrical conductivity
- Optic properties
- Absorption coefficients ➤ Rosseland and Planck mean opacities;

Accuracy of all DFT-predicted properties depends on the reliability of the XC density functional

The great majority of DFT simulations use a zero-T XC functional



We are developing advanced temperature-dependent XC functionals to improve DFT predictions in the warm dense regime

UR	
LLE	****

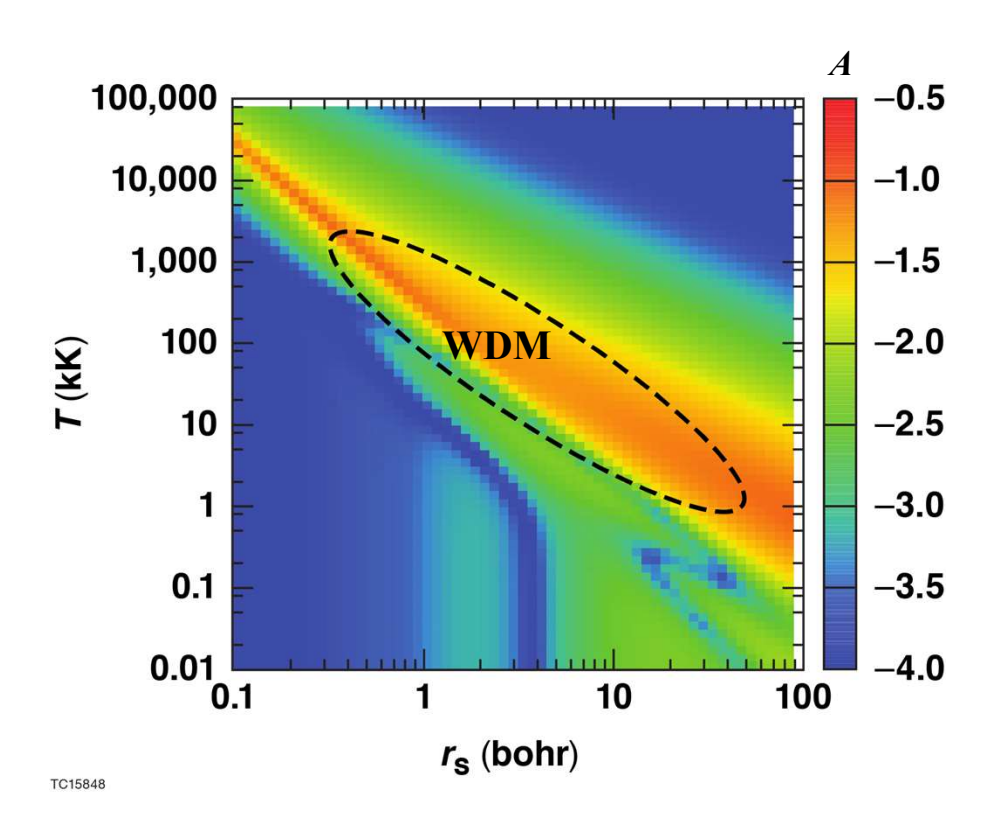
to chemical accuracy			<u>Selected</u> ground-state functionals	Thermal functionals	
Complexity	$\{oldsymbol{arphi}_i\}$	Double hybrid	XYG3, wB97X-2, wB97M LS1DGH-PBE, B2PLYP		
	ε_x	Hybrid GGA Hyper-meta-GGA	B3LYP, B97, PBE0, HSE06, TPSSh, M06-2X	KDT0, RS-KDT0 Mihaylov <i>et al.</i> , Phys. Rev. B <u>101</u> , 245141 (2020)	
	$oldsymbol{ au}$ or $ abla^2 ho(oldsymbol{r})$	meta-GGA	TPSS, SCAN, M06-L, τ-HCTH, TM	T-(r ²)SCAN(-L) [†] , <i>f</i> TSCAN Karasiev <i>et al.</i> , Phys. Rev. B <u>105</u> , L081109 (2022)	
	$ abla ho(m{r})$	GGA	PW91, BP86, PBE, BLYP, HCTH93	KDT16 Karasiev <i>et al.</i> , Phys. Rev. Lett. <u>120</u> , 076401 (2018)	
	$\rho(r)$	LDA	CA, PZ, PW, VWN	KSDT/corrKSDT, GDSMFB References below	
Fror	n Hartree-Fock t	heory	†thermalization at lower rung -L: with Laplacian dependence (deorbitalized)		

GDSMFB: Groth *et al.*, Phys. Rev. Lett. <u>119</u>, 135001 (2017) KSDT: Karasiev *et al.*, Phys. Rev. Lett. <u>112</u>, 076403 (2014)



Most quantum MD simulations use T = 0 XC functionals, which do not take into account XC thermal effects; Our calculations show the importance of these effects for HEG in the warm dense regime





$$\begin{array}{ccc} f_{xc}(r_s,T) & - \text{ XC LDA free} - \text{energy per particle,} \\ & \text{KSDT parameterization quantum Monte-Carlo (QMC)} \\ \text{data} \end{array}$$

$$\epsilon_{xc}(r_s)$$
 — XC zero — T LDA energy per particle,
Perdew — Zunger (1981) parameterization;
 $f_s(r_s,T)$ — non — interacting free — energy per particle;

$$A = \log \left(\frac{|f_{xc}(r_s, T) - \varepsilon_{xc}(r_s)|}{|f_s(r_s, T)| + |\varepsilon_{xc}(r_s)|} \right) - \text{ measure of importance of the explicit } T - \text{dependence in XC free} - \text{energy.}$$



GGA rung: We developed a framework for *T*-dependent XC GGA functional to address the issue of combined thermal and non homogeneity effects



Generalized gradient approximation (GGA)

eXchange:

Correlation:

XC thermal effects

$$F_{\mathbf{x}}^{\text{GGA}}[n,T] = \int n f_{\mathbf{x}}^{\text{LDA}}(n,T) F_{\mathbf{x}}(s_{2\mathbf{x}}(T)) d\mathbf{r}$$

$$F_{\rm c}^{\rm GGA}[n,T] = \int n f_{\rm c}^{\rm GGA}(n,\nabla n,T) d\mathbf{r}$$

XC nonhomogeneity effects

$$F_{x}(s_{2x}) = 1 + \frac{\nu_{x}s_{2x}}{1 + \alpha |s_{2x}|}$$

$$s_{2x}(n, \nabla n, T) \equiv s^2(n, \nabla n)\tilde{B}_x(t); \quad s = \frac{1}{2(3\pi^2)^{1/3}} \frac{\nabla n}{n^{4/3}}$$

$$f_{\rm x}^{\rm LDA}(n,T) = \varepsilon_{\rm x}^{\rm LDA}(n)\tilde{A}_{\rm x}(t)$$
 ; $t = T/T_{\rm F}$

GGA correlation energy per particle:

$$f_{\rm c}^{\rm GGA}(n,\nabla n,T) = f_{\rm c}^{\rm LDA}(n,T) + H(f_{\rm c}^{\rm LDA},q_{c}(T))$$

$$q_c(n, \nabla n, T) \equiv q(n, \nabla n) \sqrt{\tilde{B}_c(n, t)}$$

<u>Imposed constraints on exchange and correlation:</u>

- Reproduce finite-T small-s gradient expansion
- Satisfy Lieb–Oxford bound at T = 0
- Reduces to the correct T = 0 limit
- Reduces to the correct high-T limit

V. V. Karasiev, J. W. Dufty, and S. B. Trickey, Phys. Rev. Lett. 120, 076401 (2018).



Meta-GGA additive: The T-SCAN-L XC functional includes thermal effects at the GGA level via additive thermal correction combined with a ground-state meta-GGA



 The T-SCAN-L functional is based on the inclusion of GGA-level thermal effects with the ground-state Laplacian-level (deorbitalized) SCAN-L functional via an additive correction:

$$\mathcal{F}_{xc}^{\text{meta-GGA}}[n,T] = E_{xc}^{\text{meta-GGA}}[n] + \Delta \mathcal{F}_{xc}^{\text{GGA}}[n,T]$$

 Thermal effects at the GGA level are calculated from the difference between fully thermal (KDT16) and ground state (PBE) energies:

$$\Delta \mathcal{F}_{\mathrm{xc}}^{\mathrm{GGA}}[n,T] = \mathcal{F}_{\mathrm{xc}}^{\mathrm{KDT16}}[n,T] - E_{\mathrm{xc}}^{\mathrm{PBE}}[n]$$

However, such deorbitalized functionals feature persistent drawbacks in handling complex chemical systems.
 One such example is the artificial solidification of water at ambient conditions.



The fully-thermal meta-GGA: fTSCAN replaces input variables (isoorbital indicator α , reduced density gradients s and q) with versions including proper thermal dependence.



SCAN

fTSCAN

LDA exchange and correlation energies per particle

$$\varepsilon_x^{LDA}(n), \varepsilon_c^{LDA}(n), \varepsilon_c^{LDA0}(n)$$

$$f_x^{KSDT}(n,T), f_c^{KSDT}(n,T), f_c^{LDA0+KSDT}(n,T)$$

Reduced density gradient for exchange

$$s(n, \nabla n) = \frac{|\nabla n|}{2k_F n}$$

$$s_{2x}(n, \nabla n, T) = s^2(n, \nabla n) \frac{\widetilde{B_x}(t)}{\widetilde{A_x}(t)}$$

Reduced density gradient for correlation

$$q(n, \nabla n) = \frac{|\nabla n|}{2k_s n}$$

$$q_c(n, \nabla n, T) = q(n, \nabla n) \sqrt{\widetilde{B_c}(r_s, t)}$$

Isoorbital indicator α (including KS, Thomas-Fermi, and von Weiszäcker KED)

$$lpha(n,
abla n, au) = rac{t^{
m orb, KS} - t^{
m VW}}{t^{
m TF}}$$
 }-- Pauli KED

$$\alpha_T(n, \nabla n, \tau, T) = \frac{\tau^{\text{orb}, MKS} - t^{VW}}{t_{TF}\xi(t)}$$

Thermal variables $\xi(t)$, $\widetilde{A_x}(t)$, $\widetilde{B_x}(t)$, $\widetilde{B_c}(r_s,t)$ are built from the finite-T extension of the XC gradient expansion for weakly inhomogenous density and are valid for any temperature.

The fully-thermal *f*TSCAN functional improves the description of thermal effects up to the meta-GGA level while avoiding the shortcomings of deorbitalization.

Karasiev, V.V., *et al.* (2014) *Phys. Rev. Lett.* 112, 076403 Karasiev, V. V.; Dufty, J.; Trickey, S.B. (2018) *Phys. Rev. Lett.* 120, 076401



Global Hybrid XC Functionals



- LDA and GGA functionals suffer from self-interaction error, leading to band gap underestimation.
- HF theory removes self-interaction error but neglects correlation, overestimating band gaps.
- Hybrid functionals mix a portion of HF exchange with DFT exchange-correlation to balance accuracy.
 - Full correlation $E_x^{GGA}[n]$ Fraction of $E_x^{HF}[n]$ Fraction of $E_x^{HF}[n]$ Global Hybrid
- Global hybrids (e.g., PBE0) improve upon LDA/GGA, especially for band gaps.
- Limitations:
 - Computationally expensive due to long-range Coulomb interactions
 - Still slightly overestimates band gaps in some semiconductors



KDT0 is a finite-*T* extension to PBE0 in a sense that it includes explicit *T* dependent components.



PBE0*:
$$F_{xc}^{PBE0}[n,T] = E_{xc}^{PBE}[n] + \frac{1}{4} \left(E_x^{HF}[n,T] - E_x^{PBE}[n] \right)$$

KDT0**:
$$F_{xc}^{\text{KDT0}}[n,T] = F_{xc}^{\text{KDT16}}[n,T] + \frac{1}{4} \left(F_{x}^{\text{HF}}[n,T] - F_{x}^{\text{KDT16}}[n,T] \right)$$



^{*} J. P. Perdew, M. Ernzerhof, and K. Burke, J. Chem. Phys. <u>105</u>, 9982 (1996).

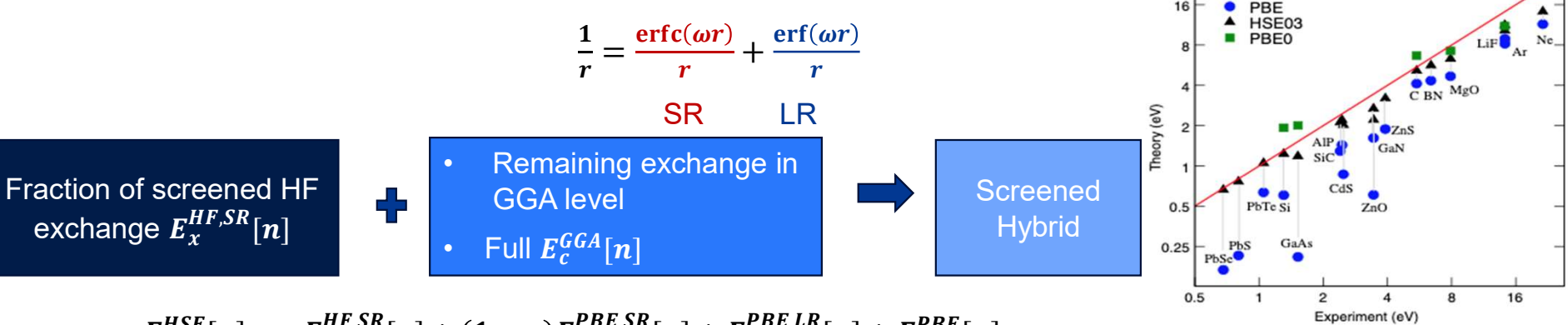
^{**} D. Mihaylov, V. V. Karasiev, and S. X. Hu, Physical Review B 101 (24), 245141 (2020).

Range-Seperated (screened) Hybrid functional



- In solid state physics HF has unphysical implication in metallic system calculation due to 1/r asymptotic behavior.
- It turns out that screening effect is necessary.

The range-separated hybrid functional is developed by dividing the coulomb potential into short and long range parts where the separation is controlled by ω



 $E_{xc}^{HSE}[n] = aE_{x}^{HF,SR}[n] + (1-a)E_{x}^{PBE,SR}[n] + E_{x}^{PBE,LR}[n] + E_{c}^{PBE}[n]$

M Marsman et al 2008 J. Phys.: Condens. Matter 20 064201

Our goal is to develop thermal RS hybrid XC functional which extends the accuracy of HSE to WDM regime



Range-Seperated Hybrid functional (RS-KDT0)



Fraction of screened HF exchange $\mathcal{F}_{x}^{HF,SR}[n,T]$



- Remaining exchange in thermal GGA level
- Full $\mathcal{F}_c^{GGA}[n,T]$



Screened Hybrid (RS-KDT0)

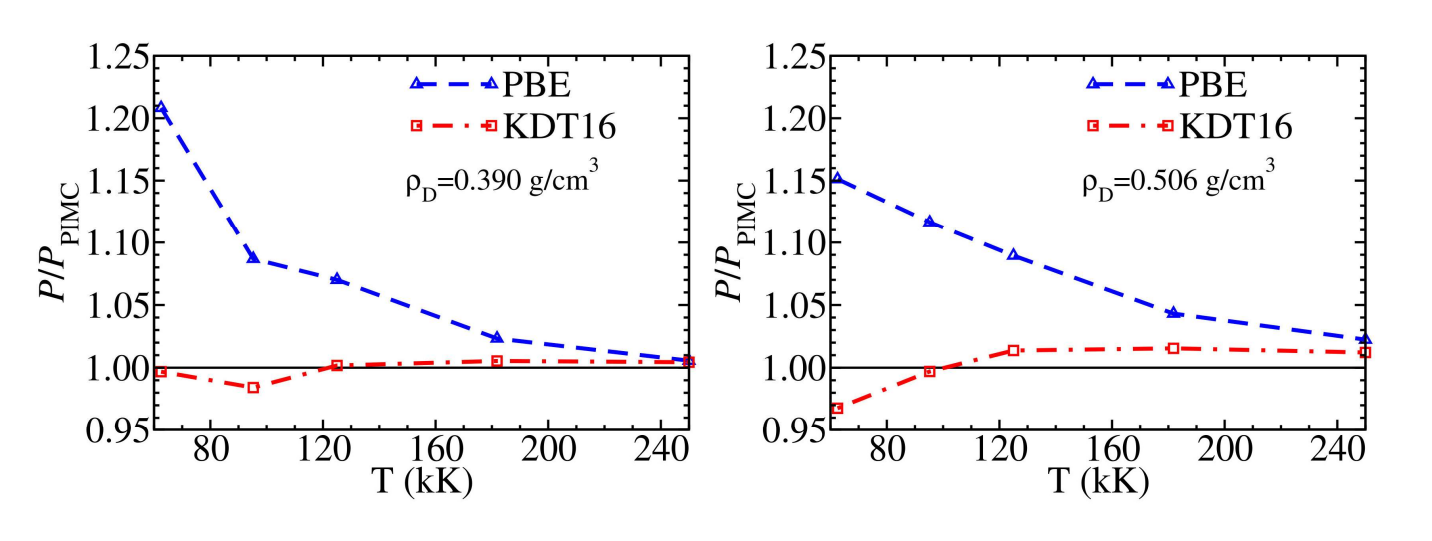
- RS-KDT0 is constructed to satisfy the following limiting behavior:
 - In the limit $T \rightarrow 0$, RS-KDT0 reduces closely to ground state HSE functional
 - For $\omega = 0$, RS-KDT0 reduces to global hybrid KDT0
 - In the limit $\omega \to \infty$, the thermal Hartree-Fock exchange vanishes due to complete screening, and RS-KDT0 reduces to the thermal GGA functional KDT16
- RS-KDT0 takes the following form

$$\mathcal{F}_{xc}^{RS-KDT0}[n,T] = a\mathcal{F}_{x}^{HF,SR}[n,T] + (1-a)\mathcal{F}_{x}^{KDT16,SR}[n,T] + \mathcal{F}_{x}^{KDT16,LR}[n,T] + \mathcal{F}_{c}^{KDT16}[n,T]$$



Results -- thermal GGA: Relative error of pressure is significantly reduced (as compared to the ground-state PBE) when KDT16 is applied to EOS of warm-dense D

- Path-integral Monte Carlo (PIMC) data at high-T are used as a reference
- KDT16 provides excellent agreement with regard to the PIMC reference



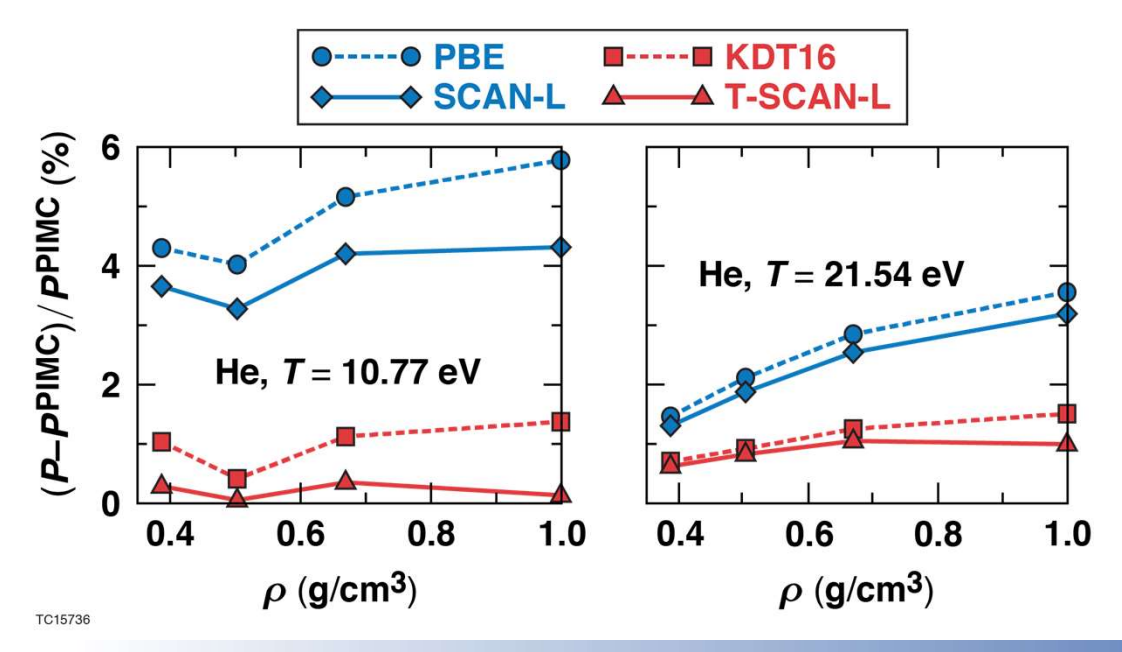
← The relative error of electronic pressure from DFT simulations with respect to the reference PIMC results

*S.X. Hu, B. Militzer, et al., Phys. Rev. B 84, 224109 (2011).



Results -- thermal GGA and meta-GGA-additive: Relative error of pressure is reduced by a factor of 3 to 10 when T-SCAN-L is applied to EOS of warm-dense He

- Path-integral Monte Carlo (PIMC) data at high-T are used as a reference
- KDT16 and T-SCAN-L (meta-GGA + thermal) provide excellent agreement with regard to the PIMC reference



← The relative error of total pressure from DFT simulations with respect to the reference PIMC results

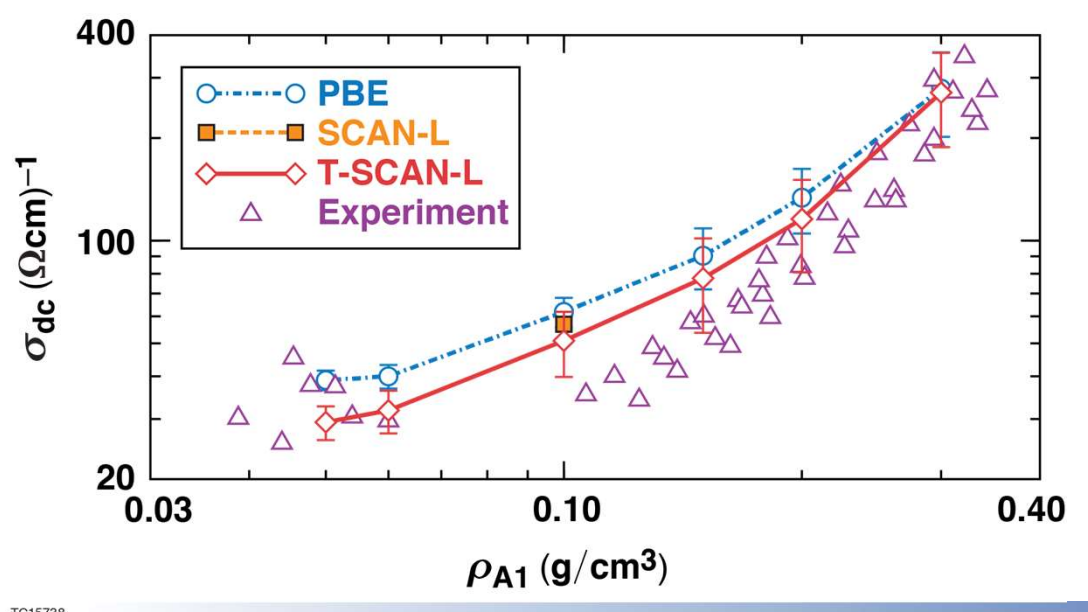


^{*}B. Militzer, Phys. Rev. B 79, 155105 (2009).

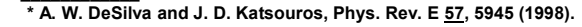
Results -- thermal GGA and meta-GGA-additive: Application of KDt16 and T-SCAN-L to dc conductivity of warm-dense Al shows better agreement w/r to experimental measurements



- Thermal KDT16 andT-SCAN-L functional improves the accuracy of transport property predictions as compared to standard ground-state functionals
- Thermal hybrid XC (KDT0 and RS-KDT0) are expected to improve accuracy as compared to the above semi-local functionals



← Al dc conductivity as a function of density along *T* = 10,000 K isotherm

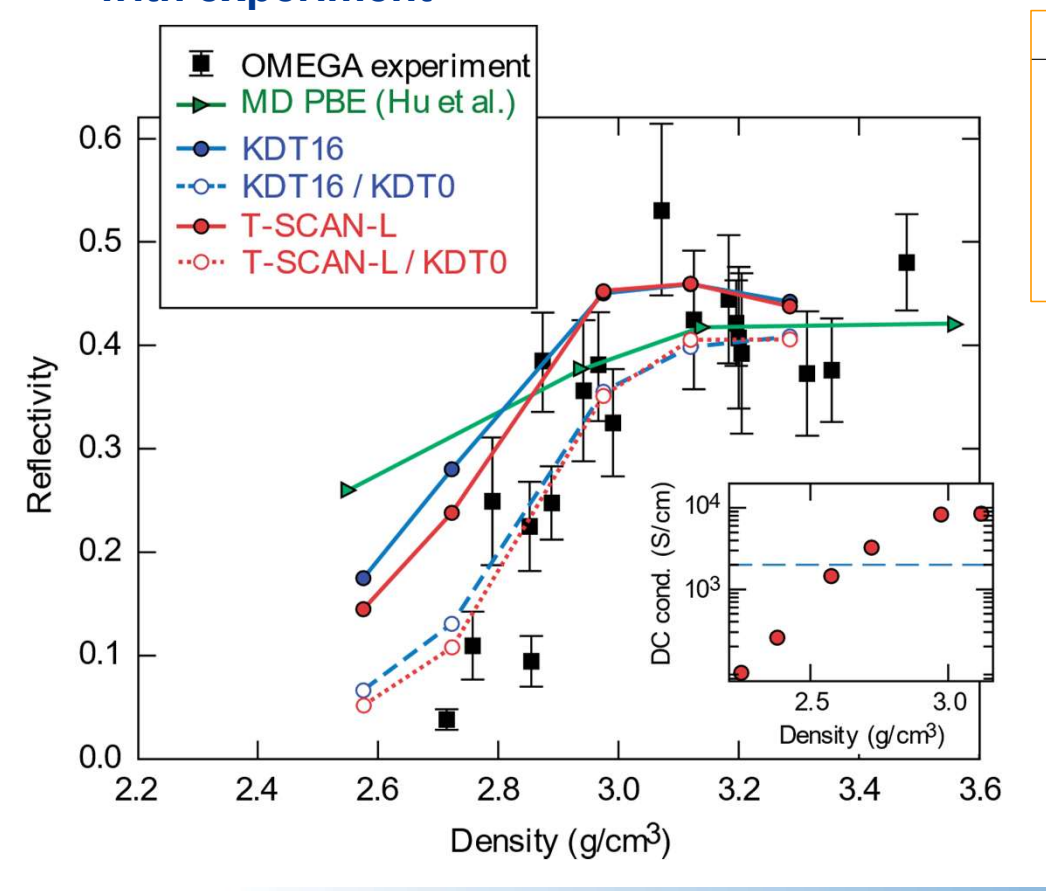




Results – CH optical properties

Insulator-metal transition boundary along the principal Hugoniot predicted by SCANL/KDT0 XC and indicated in sudden jump of reflectivity and dc conductivity are in better agreement

with experiment



PHYSICAL REVIEW B 107, 155116 (2023)

Shock-induced metallization of polystyrene along the principal Hugoniot investigated by advanced thermal density functionals

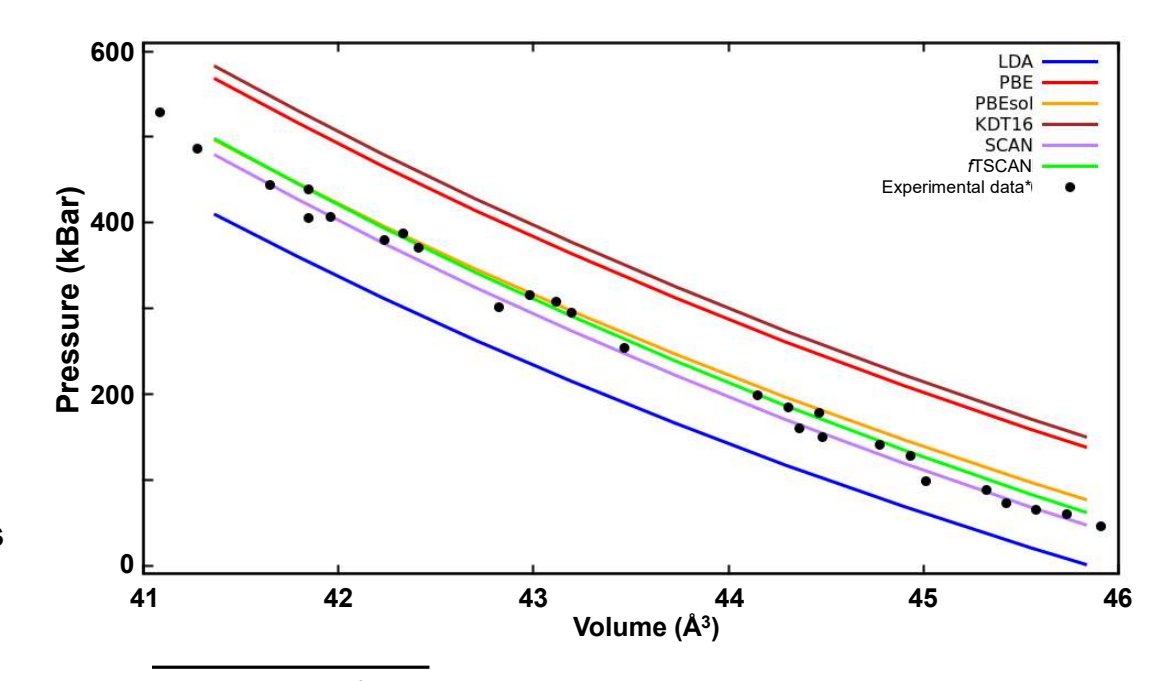
R. M. N. Goshadze, Valentin V. Karasiev ,* D. I. Mihaylov , and S. X. Hu Laboratory for Laser Energetics, University of Rochester, 250 East River Road, Rochester, New York 14623-1299, USA

- T-SCAN-L shifts reflectivity turn-on point to the right and making the curve sharper as compared to PBE and in agreement with experiment
- The insets show dc conductivity. The jump in dc conductivity is in correspondence with the jump in reflectivity indicating the IMT boundary



Meta-GGA-level functionals exhibit improved correspondence with experimental lattice constants compared to LDA or GGA; fTSCAN preserves accuracy of SCAN

- Experimental P-V data for cold SiO₂ (stishovite) is poorly modeled by LDA, PBE, and KDT16 functionals.
- Meta-GGA functionals SCAN and fTSCAN provide an excellent match to experimental data.
 - Note: PBEsol, a GGA-level functional parameterized for improved lattice constants, also matches experimental data well.
- Improvements in modeling complex systems favor the use of meta-GGA XC functionals from ambient to WDM conditions.
- At elevated temperatures fTSCAN provides very similar improvements of accuracy as thermal KDT16 and TSCANL



Experimental data from:
Fischer, R. A., et al. (2018) Am. Min. 103, 792-802
Andrault, D., et al. (2003) Am. Min. 88, 301-307
Grocholski, B., et al. (2013) J. Geophys. Res.: Solid Earth 118, 1-13
Hemley, R. J., et al. (2000) Solid State Commun. 114, 527-532
Ross, N. L., et al. (1990) Am. Min. 75, 739-747



Band gap calculations for semi-conductors at ambient conditions



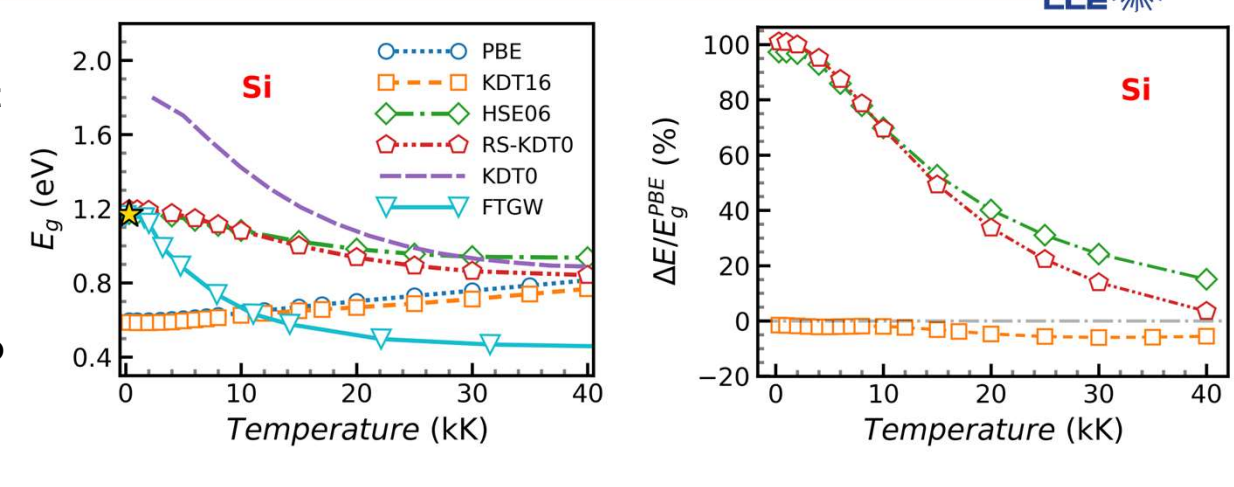
System	Lattice Constant (Å) [1]	PBE BG (eV)	KDT0 BG (eV)	HSE06 BG (eV)		Experiment (eV) [1]
C	3.567	4.15	6.05	5.33	5.36	5.48
Ge	5.658	0.06	1.32	0.8	0.81	0.74
GaAs	5.648	0.6	1.98	1.44	1.45	1.52
InSb	6.479	0	1.01	0.53	0.54	0.23

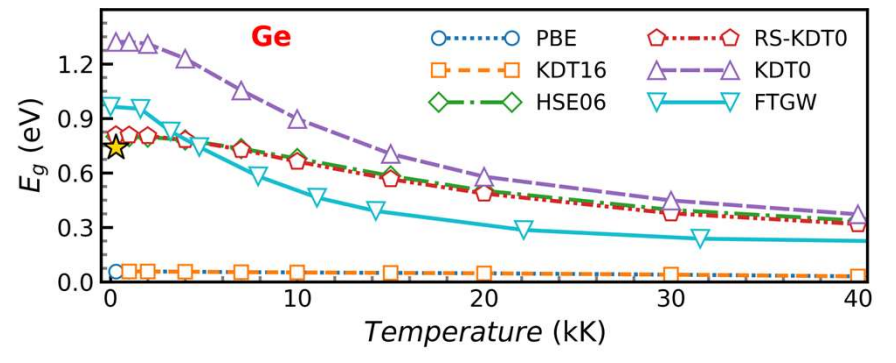
- RS-KDT0 matches HSE06 at room temperature, as expected
- PBE underestimates band gaps in semiconductors, sometimes predicts metallic behavior (Ge and InSb)
- RS-KDT0 shows better agreement with experiments than KDT0, Inherits HSE06 accuracy in the lowtemperature regime



Benchmarking RS-KDT0: Si and Ge (semi-conductors)

- RS-KDT0, HSE06, and FT-GW show strong agreement with experimental band gaps at low temperatures.
- At temperatures above 20,000 K, thermal effects from GGA become significant, reducing the RS-KDT0 band gap relative to HSE06 and bringing it closer to FT-GW.
- GGA limitations are evident in Ge, where PBE and KDT16 incorrectly predict a metallic state.







Applications

Accurate knowledge of H/He/H-He properties (EOS/transport etc.) is crucial for modeling giant planetary interiors



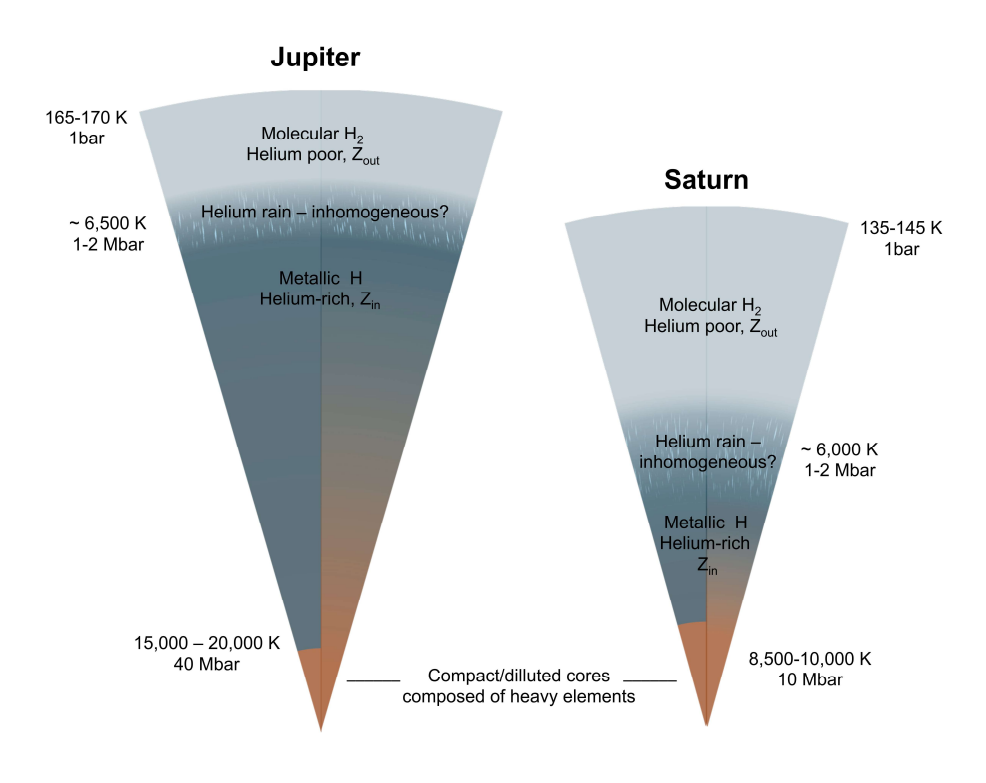


Figure 5. Sketches of the internal structures of Jupiter and Saturn.

R. Helled, ArXiv 1812.07436v1 (2018) S. Howard, S. M\:uller, and R. Helled, A&A, <u>689</u>, A15 (2024)



The most successful approach up to date is based on evaluation of the Gibbs free energy of mixing and corresponding double-tangent construction^{1,2}

The free enthalpy (Gibbs free energy) of mixing ΔG is given by:

$$\Delta G(x, P, T) = G(x, P, T) - xG(1, P, T) - (1 - x)G(0, P, T)$$

Where G is the free enthalpy as a function of He fraction, x, pressure, P, and temperature, T:

$$G(x,P,T) = U(x,P,T) - TS(x,P,T) + PV(x,P,T)$$

G(x,P,T) in first equation requires to be the free enthalpy of a perfectly mixed system (to avoid any double counting contributions into ΔG . There are contradictory conditions for this requirement:

- from one side the system must be small enough to avoid any possible mixing;
- from another side the system has to be large enough to reduce finite-size effects;

Heating of the system along an isobar involves two processes, H-He demixing/mixing and H₂ atomization (-> insulator-to-metal transition (IMT):

it is not clear how accurately the H₂ atomization process is treated in simulation with very small simulation cell, less than 32 H₂ molecules; overall the demixing temperature might be affected by this procedure

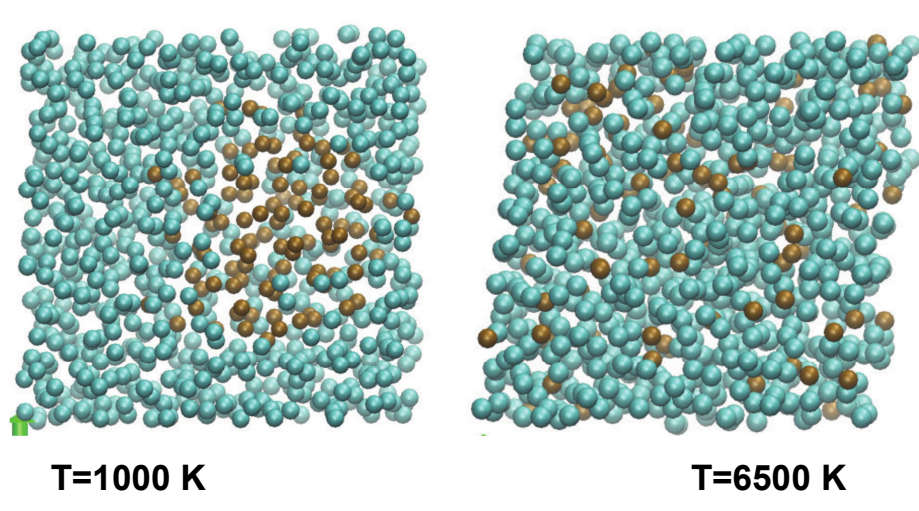
This method does not provide any insights on structural and transport properties of the system

¹Lorenzen et al., PRL 102, 115701 (2009)

²Sh\:ottler et al., PRL 120, 115703 (2018)



Analyzing large-cell AIMD simulations snapshots, it is easy to see that H-He demixing occurs directly in the simulation box: He₁₀₄H₈₁₆ (1024e⁻), KDT16, *P*=150 GPa



- The H-He interface in demixed 2-phase state is a surface, hence the first peak in the He-H RDF should be depressed as compared to the perfectly mixed system when the H-He interface is "volumetric"
- We found that the magnitude of the first peak in the He-H RDF provides a sharp quantitative signature of the H-He demixing/mixing



Qualitative features of the H-H, He-He, and H-He RDFs at demixed 2-phase state: He₁₀₄H₈₁₆ (1024e⁻), KDT16, *P*=150 GPa

- the probability for a He atom to find a H atom at low is reduced as compared to the perfectly mixed system when the H-He interface is "volumetric"
- the probability of He atoms being close to H atoms at large distances is enhanced (greater than 1) compared to the perfect mixture
- the probability for H/He atoms to be close to an atom of the same species at large distances is reduced, H-H and He-He RDFs at large distances drop below 1, while these values are equal to one in the case of nearperfect mixing
- the probability for H/He atoms to be close to an atom of the same species at low distances is enhanced as compared to the perfectly mixed system

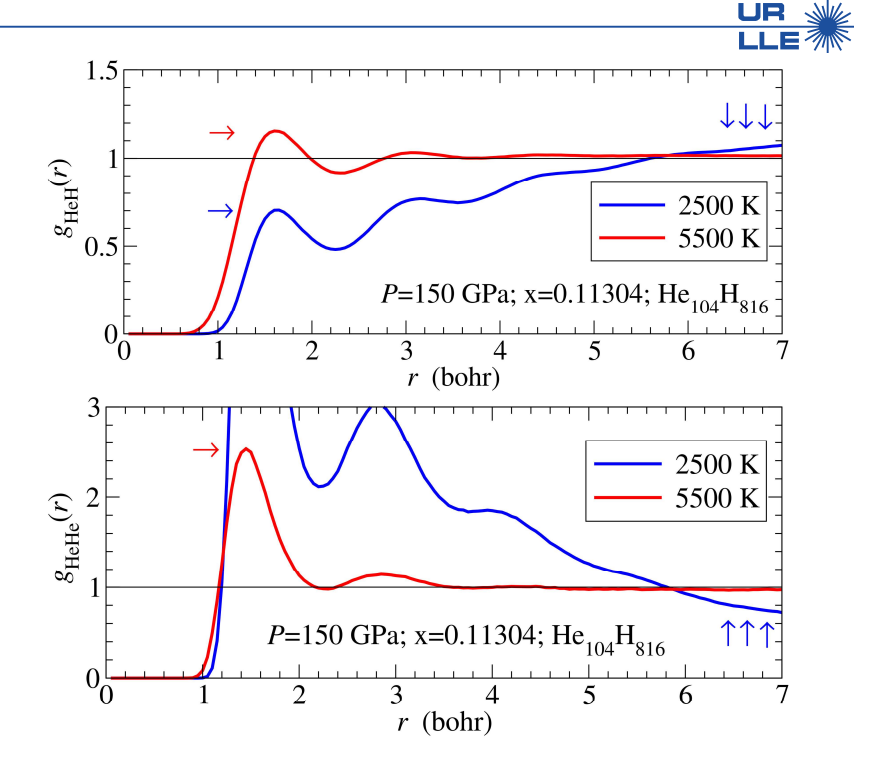
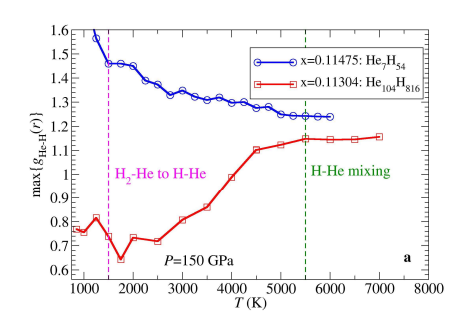


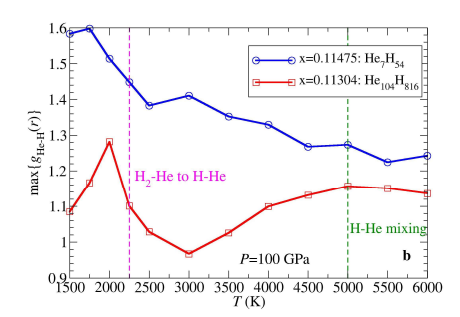
FIG. S1: Features of the He-H and He-He RDFs indicating the demixing process. Two examples are shown for a H-He (${\rm He_{104}H_{816}},\,x_{\rm He}=0.11304$) mixture at a pressure of 150 GPa and temperatures of 2500 K and 5500 K corresponding to a demixed and mixed state, respectively.

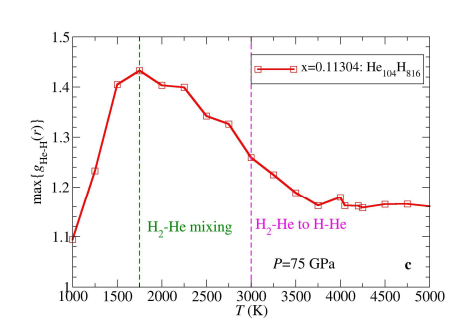


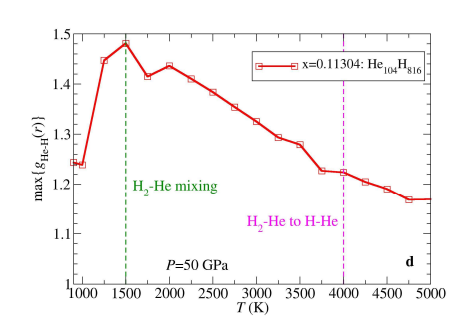
Increase of the He-H RDF first peak along selected isobar for an atomic He fraction x=0.11 clearly indicates the transition to the mixed state









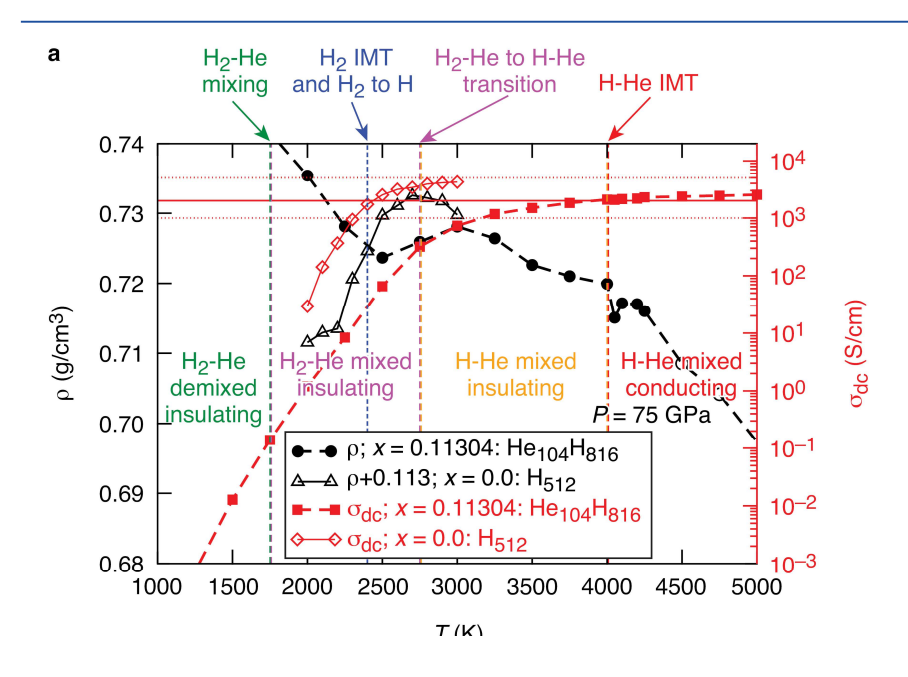


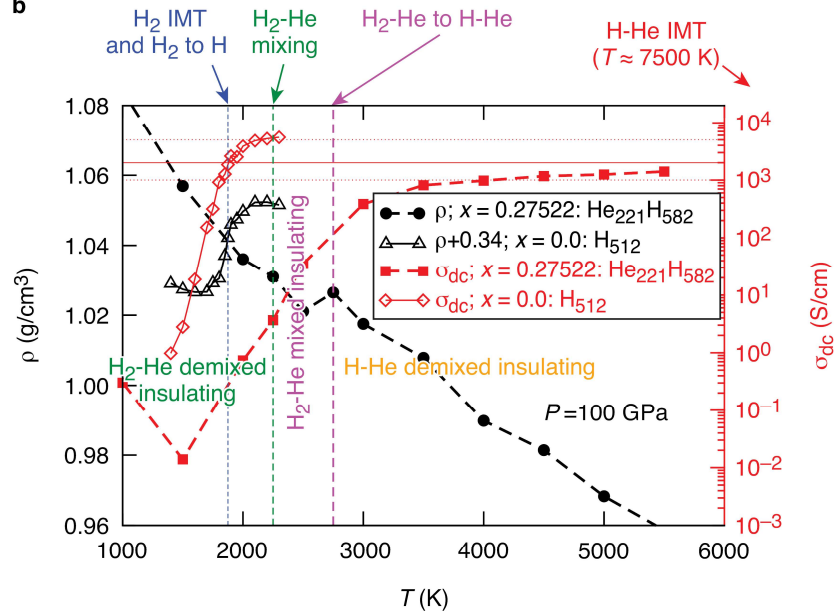
- At low-T the He-H RDF first peak in large system (red curve) is lower as compared to the small perfectly mixed system, indicating demixing
- Metallization of H₂ subsystem upon atomization (at 1500 K and 2250 K) is not the primary driver, albeit it forces the H-He demixing process
- The He-H RDF first peak reaches the maximum indicating the transition to mixed state (vertical dashed green lines)



Structural properties and static electrical conductivity of H-He mixtures







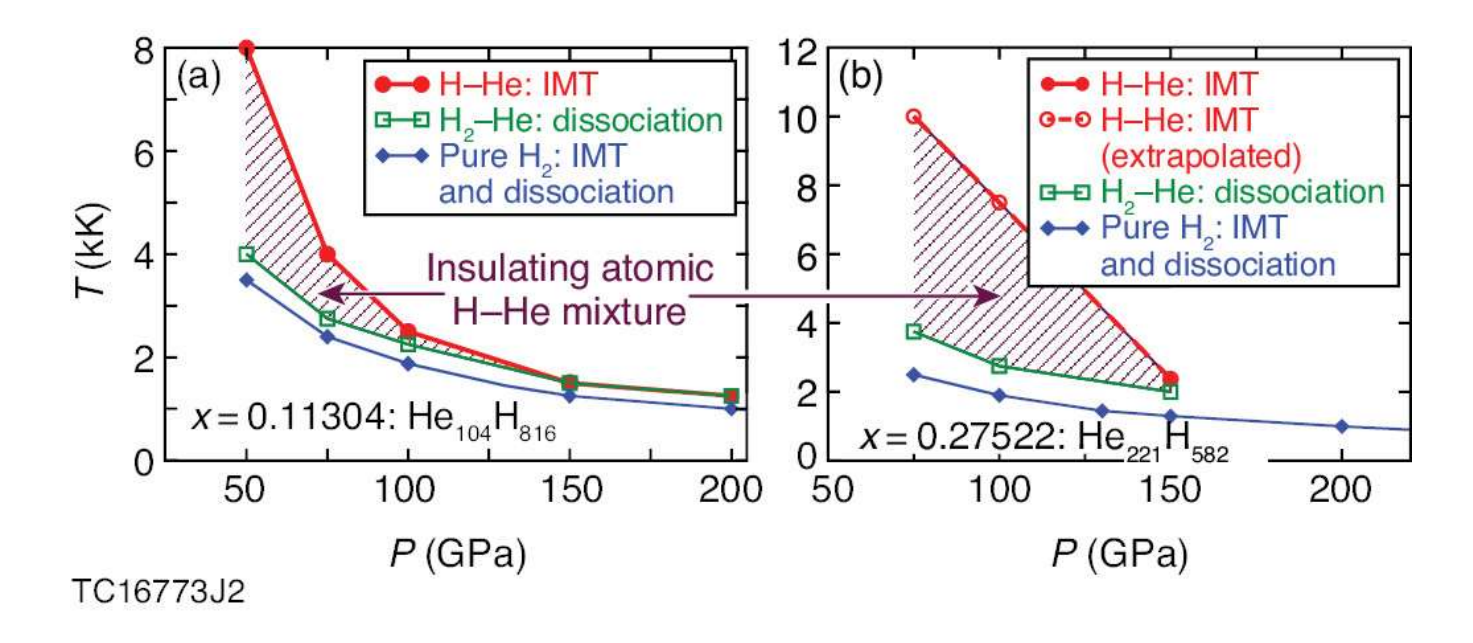
Density and dc conductivity of H-He mixtures as compared to pure H:

- a. Density and dc conductivity profiles along the P = 75 isobar indicating temperatures of the H_2 -He \Rightarrow H-He, IMT and H-He demixing/mixing transitions in liquid $H_{204}H_{816}$ (x=0.11304) as predicted by DFT simulations with advanced thermal KDT16 XC.
- b. Same as in a for $He_{221}H_{582}$ (x=0.27522) mixture.



The offset of insulator-metal transition relative to the H subsystem dissociation in H-He mixtures



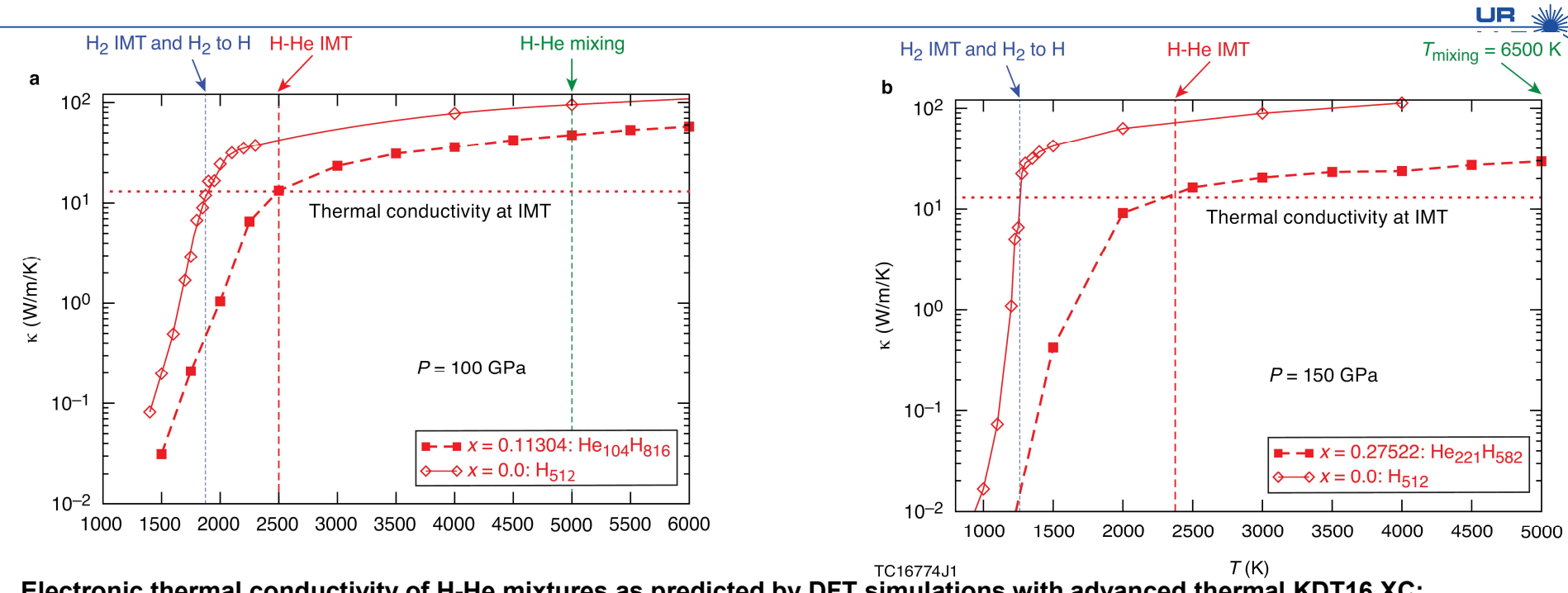


a: H-He mixture insulator-metal transition and H_2 -He \rightarrow H-He dissociation curves for the $He_{104}H_{816}$ (x=0.11304) mixture are compared to the IMT and dissociation boundary of pure H_2 .

b: Same as in a for $He_{221}H_{582}$ (x=0.27522) mixture. Both panels show a wide range of thermodynamic conditions when atomic H - He mixture is insulating.



Structural properties and static thermal conductivity of H-He mixtures



Electronic thermal conductivity of H-He mixtures as predicted by DFT simulations with advanced thermal KDT16 XC:

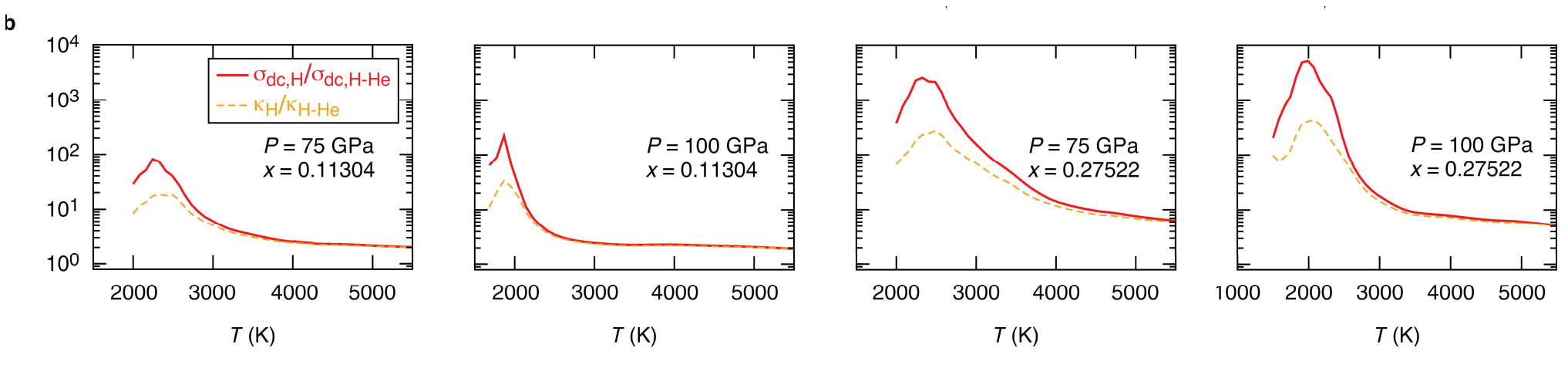
a: Liquid $He_{104}H_{816}$ mixture (x=0.11304) along P = 100 GPa. Comparisons are made to the pure H system. Horizontal dashed line shows a near-universal value (≈ 13 W/m/K) of the electronic thermal conductivity reached upon the insulator-metal transition for each system.

B: Liquid $He_{221}H_{582}$ mixture (x=0.27522) along P = 100 GPa isobar.



Static electrical and thermal conductivities of H-He mixtures are drastically reduced as compared to pure H properties





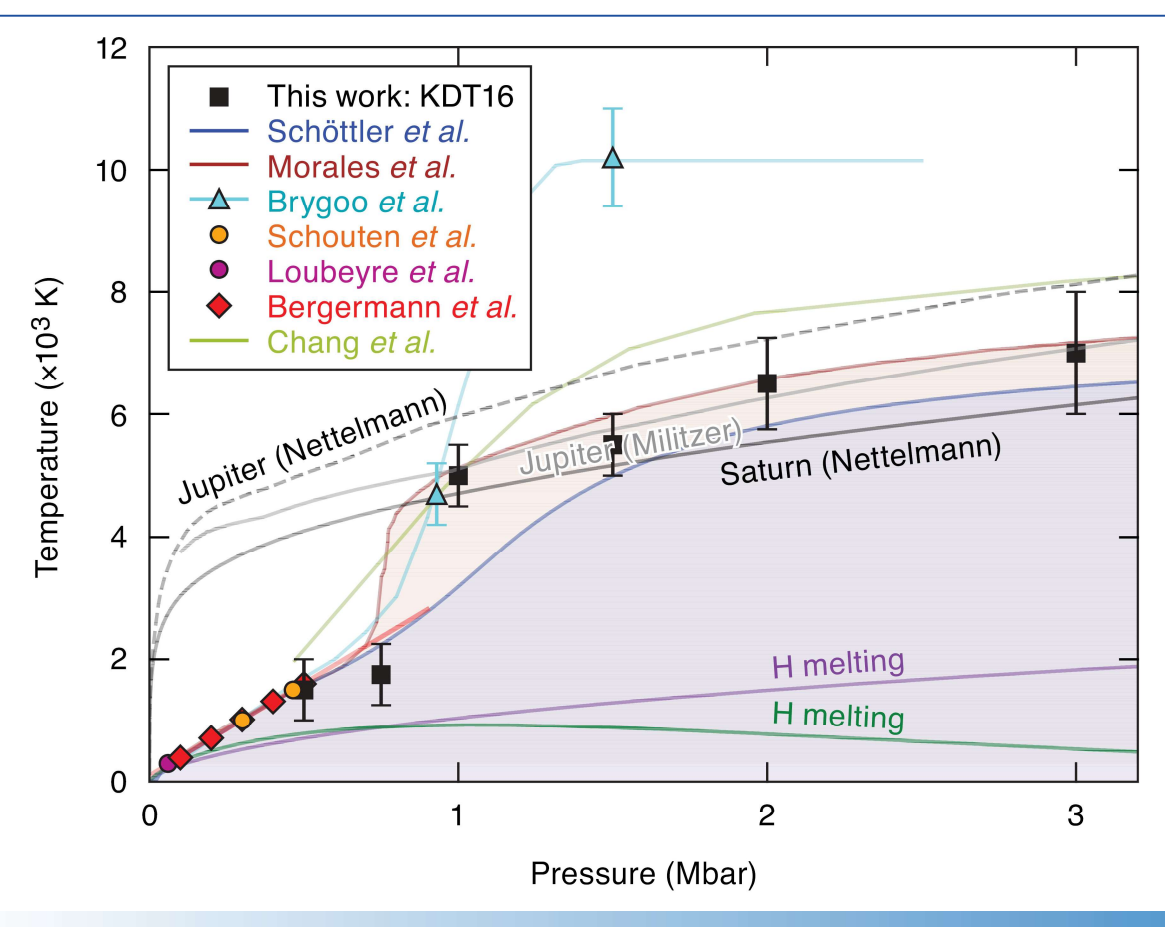
Density and dc conductivity of H-He mixtures as compared to pure H:

- a. Density and dc conductivity profiles along the P = 75 isobar indicating temperatures of the H_2 -He \Rightarrow H-He, IMT and H-He demixing/mixing transitions in liquid $H_{2104}H_{816}$ (x=0.11304) as predicted by DFT simulations with advanced thermal KDT16 XC.
- b. Same as in a for $He_{221}H_{582}$ (x=0.27522) mixture.



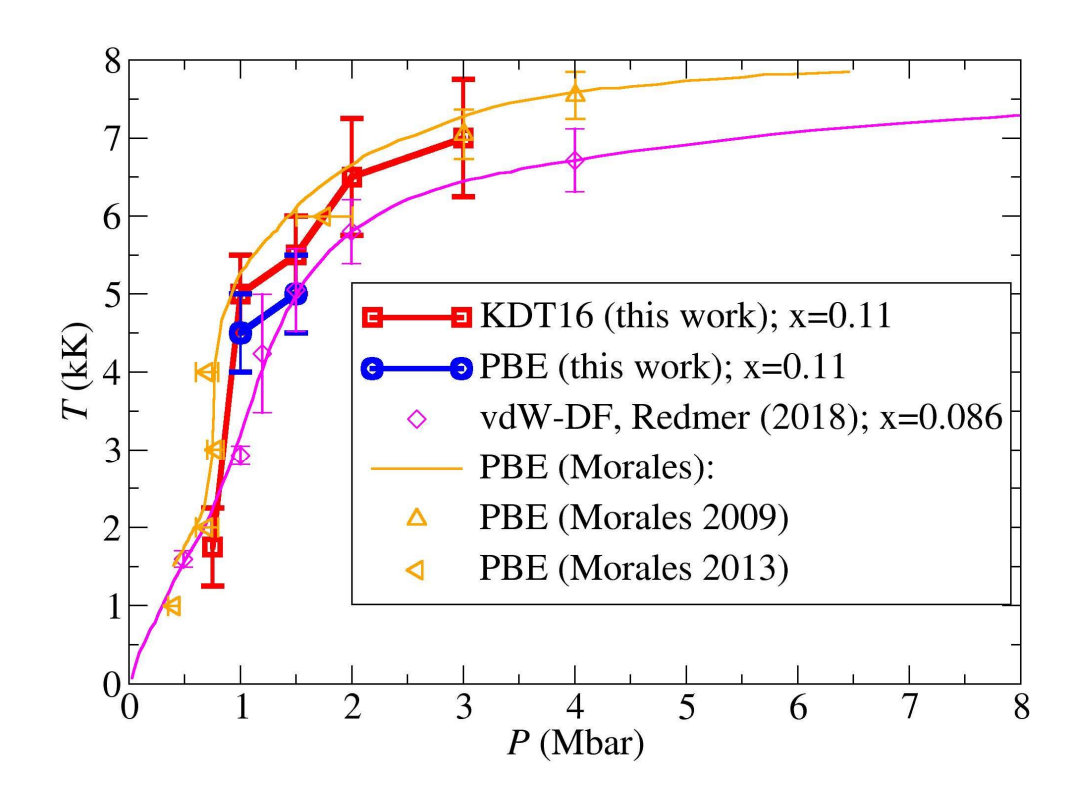
Miscibility diagram for solar He abundance







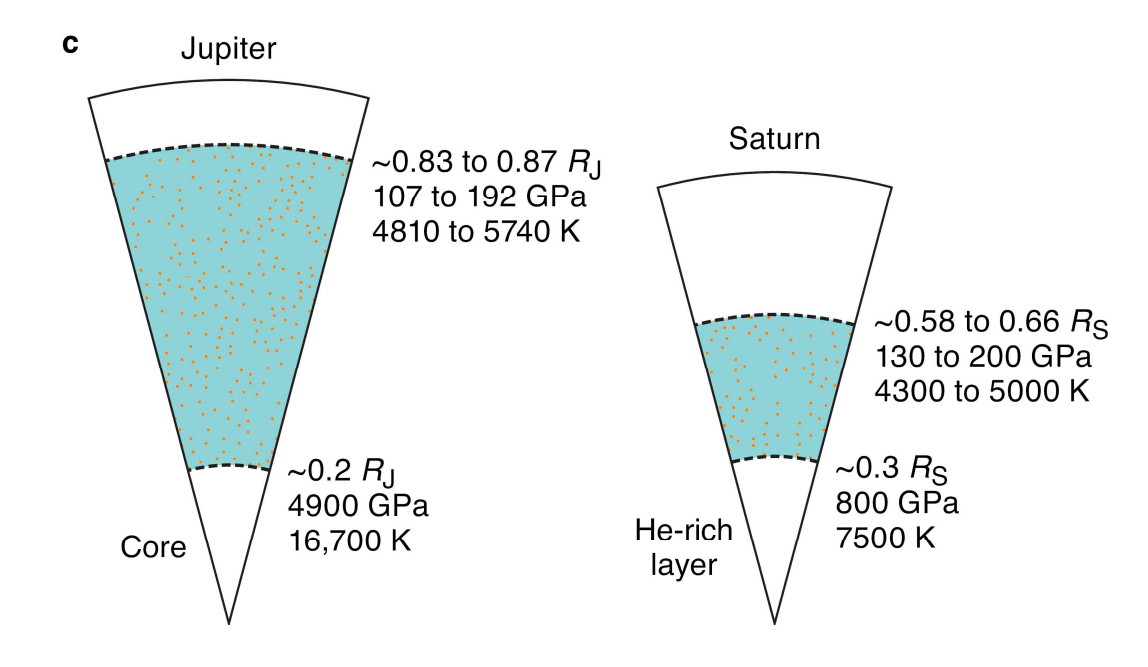
H-He miscibility boundary as identified by thermal XC functional is located about 500 K higher as compared to the ground-state XC functional predictions (PBE our work and vdW-DF (Redmer (2018))





Estimated interior regions of Jupiter and Saturn potentially affected by reduced electrical and thermal conductivity properties of H-He mixtures





Reduced transport properties affects the planetary models prediction for the H-He demixing layer, its thickness, in particular, the stability of this layer against convection, compositional gradient, planetary gravity waves, and dynamo.



Summary

Exchange-correlation thermal effects are important in warm dense matter and dense plasma regimes and must be taken into account via thermal XC functionals for reliable DFT-based predictions



- Systematic development of thermal XC functionals at the LDA, GGA, and meta-GGA level of theory clearly demonstrate systematic improvements of the accuracy of DFT simulations in warm dense matter (WDM) and dense plasma regimes
- Thermal XC functionals can be applied across entire range of thermodynamic conditions from near-ambient to extreme given that thermal XC reduce to the ground-state XC counterparts at low-T
- The new T-dependent meta-GGA XC (T-SCAN-L and fTSCAN) in combination with thermal hybrids, are the most reliable functional across the entire temperature range, providing accurate predictions of (as demonstrated so far) for EOS of D and He, and dc conductivity of low-density Al
- New method to predict H-He demising boundary has been proposed. The method avoids finitesize effects and provide insights on structural and conducting properties of mixtures
- Offset of IMT in H-He mixture relative to the H₂ IMT has consequences for Jupiter and Saturn's thermal evolution, internal structure and dynamo

XC: exchange correlation
DFT: density functional theory
LDA: local density approximation
GGA: generalized gradient approximation

SCAN-L: de-orbitalized strongly constrained appropriately normed

Karasiev et al., PRL 112, 076403 (2014) Karasiev et al., PRL 120, 076401 (2018) Mihaylov, et al., PRB 101, 245141 (2020) Hilleke et al., PRM 9, L050801 (2025) Ellaboudy et al., PRB (2025) (under review) Karasiev, et al., PRL, (2025) (under review)

